NeuroImage 297 (2024) 120749

Contents lists available at ScienceDirect

NeuroImage

journal homepage: www.elsevier.com/locate/ynimg

Differentiating loss of consciousness causes through artificial intelligence-enabled decoding of functional connectivity

Young-Tak Kim [a,1], Hayom Kim [b,1], Mingyeong So [b], Jooheon Kong [b], Keun-Tae Kim [b], Je Hyeong Hong [c], Yunsik Son [d], Jason K. Sa [a,e], Synho Do [f,g,h], Jae-Ho Han [i], Jung Bin Kim [b,*]

[a] Department of Biomedical Sciences, Korea University College of Medicine, 73, Goryeodae-ro, Seongbuk-gu, Seoul, 02841, Republic of Korea
[b] Department of Neurology, Korea University Anam Hospital, Korea University College of Medicine, 73, Goryeodae-ro, Seongbuk-gu, Seoul, 02841, Republic of Korea
[c] Department of Electronic Engineering, Hanyang University, 222, Wangsimni-ro, Seongdong-gu, Seoul, 04763, Republic of Korea
[d] Department of Computer Science and Engineering, Dongguk University, 30, Pildong-ro 1-gil, Jung-gu, Seoul, 04620, Republic of Korea
[e] Department of Biomedical Informatics, Korea University College of Medicine, 73, Goryeodae-ro, Seongbuk-gu, Seoul, 02841, Republic of Korea
[f] Department of Radiology, Massachusetts General Hospital, Harvard Medical School, 125 Nashua Street, Suite 2210, Boston, MA, 02114, United States
[g] KU-KIST Graduate School of Converging Science and Technology, Korea University, 145, Anam-ro, Seongbuk-gu, Seoul, 02841, Republic of Korea
[h] Kempner Institute, Harvard University, 150 Western Avenue, Boston, MA, 02134, United States
[i] Department of Brain and Cognitive Engineering, Korea University, 145, Anam-ro, Seongbuk-gu, Seoul, 02841, Republic of Korea

ARTICLE INFO

Keywords:
Loss of consciousness
Functional connectivity
EEG coherence network
Graph theory
Explainable artificial intelligence

ABSTRACT

Differential diagnosis of acute loss of consciousness (LOC) is crucial due to the need for different therapeutic strategies despite similar clinical presentations among etiologies such as nonconvulsive status epilepticus, metabolic encephalopathy, and benzodiazepine intoxication. While altered functional connectivity (FC) plays a pivotal role in the pathophysiology of LOC, there has been a lack of efforts to develop differential diagnosis artificial intelligence (AI) models that feature the distinctive FC change patterns specific to each LOC cause. Three approaches were applied for extracting features for the AI models: three-dimensional FC adjacency matrices, vectorized FC values, and graph theoretical measurements. Deep learning using convolutional neural networks (CNN) and various machine learning algorithms were implemented to compare classification accuracy using electroencephalography (EEG) data with different epoch sizes. The CNN model using FC adjacency matrices achieved the highest accuracy with an AUC of 0.905, with 20-s epoch data being optimal for classifying the different LOC causes. The high accuracy of the CNN model was maintained in a prospective cohort. Key distinguishing features among the LOC causes were found in the delta and theta brain wave bands. This research advances the understanding of LOC's underlying mechanisms and shows promise for enhancing diagnosis and treatment selection. Moreover, the AI models can provide accurate LOC differentiation with a relatively small amount of EEG data in 20-s epochs, which may be clinically useful.

1. Introduction

Acute loss of consciousness (LOC) is a prevalent and high-mortality manifestation in clinical settings (Zehtabchi et al., 2013), resulting in a significant socioeconomic burden (Penberthy et al., 2005). Leading causes of LOC include nonconvulsive status epilepticus (NCSE), metabolic encephalopathy (ME), and benzodiazepine intoxication (BI) (Aguilon-Leiva et al., 2022; Campbell et al., 2023; Meierkord and Holtkamp, 2007; Shorvon, 1994; Sutter et al., 2012), each necessitating distinct treatment strategies. NCSE management prioritizes urgent

Abbreviations: AI, artificial intelligence; ARAS, ascending reticular activating system; ASM, antiseizure medication; AUC, area under the ROC curve; BI, benzodiazepine intoxication; CNN, convolutional neural network; CTC, cortico-thalamo-cortical; Dl, deep learning; EEG, electroencephalography; FC, functional connectivity; GABA, γ-aminobutyric acid; GM, graph theoretical measurement; HC, healthy control; LOC, loss of consciousness; ME, metabolic encephalopathy; ML, machine learning; NCSE, nonconvulsive status epilepticus; ROC, receiver operating characteristic; SHAP, Shapley additive explanations; XAI, explainable artificial intelligence.

* Corresponding author.
E-mail address: kjbin80@korea.ac.kr (J.B. Kim).
[1] These authors contributed equally to this work.

https://doi.org/10.1016/j.neuroimage.2024.120749
Received 8 April 2024; Received in revised form 12 July 2024; Accepted 18 July 2024
Available online 19 July 2024

antiseizure medications (ASMs) (Meierkord and Holtkamp, 2007), while recovery from ME involves correcting metabolic derangements, and BI treatment may require conservative management or antidotes like flumazenil (Zamani et al., 2022). Despite the establishment of treatment strategies for each cause of LOC, it is still difficult to differentiate the cause of LOC based solely on clinical examination findings due to common symptoms, such as persistent unresponsiveness.

Conventionally, the differential diagnosis of LOC can be determined by detailed history taking, neurological examination, laboratory tests, electroencephalography (EEG), and neuroimaging studies. Among the

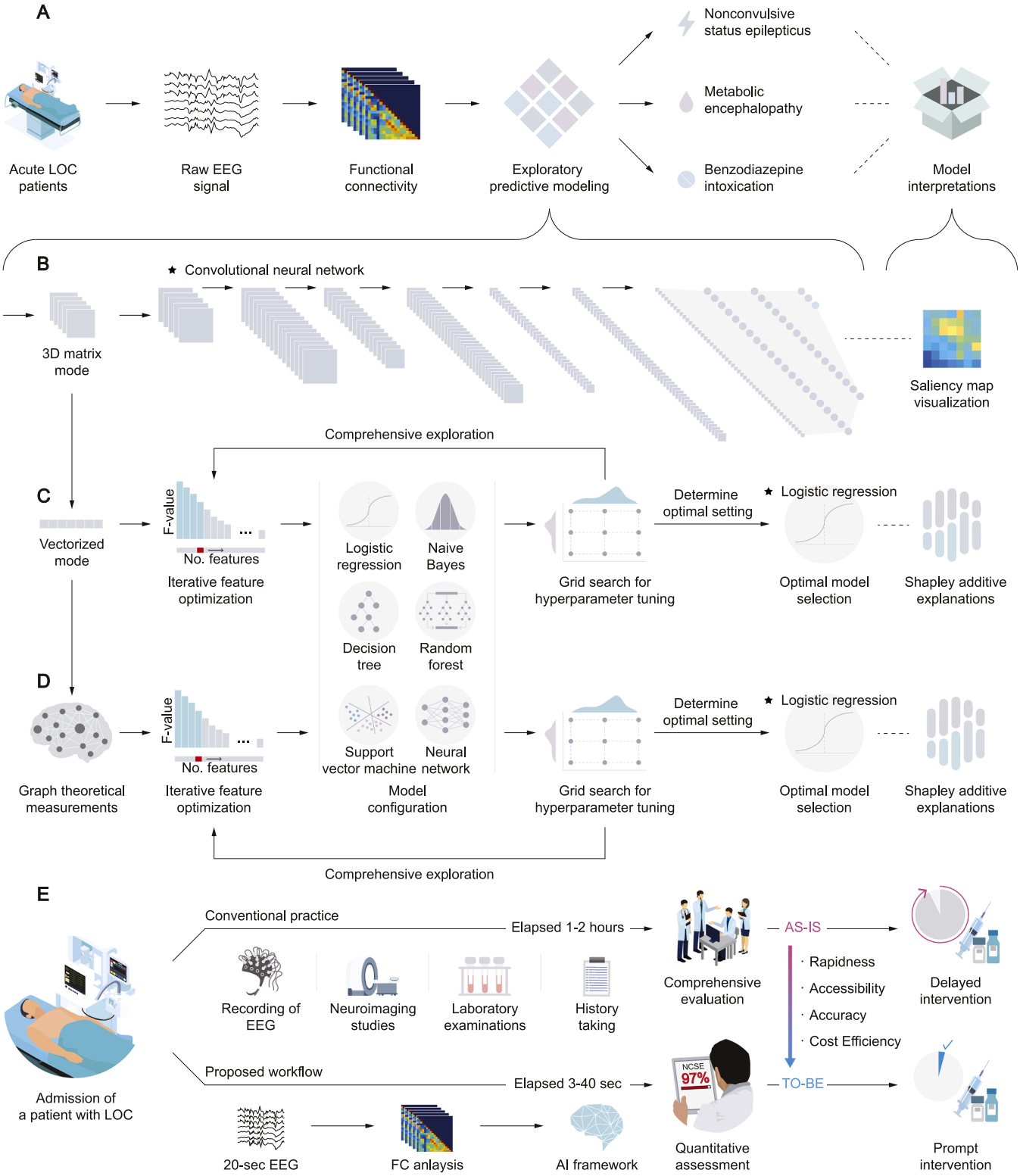

Fig. 1. AI-based study protocol for determination of the LOC causes. (**A**) End-to-end analytic workflow. (**B**) DL model using FC adjacency matrices. (**C**) ML model with vectorized FC. (**D**) ML model with GM. (**E**) Comparison between LOC management processes through conventional procedure and those using the proposed models.

diagnostic modalities, EEG can directly measure brain activity and plays a crucial role in distinguishing the causes of LOC (Leitinger et al., 2016); however, the visual interpretation process of EEG is time-consuming, laborious, dependent on significant expertise, and can be subjective (Grant et al., 2014). The development of reliable differential diagnostic models is required for the precise and rapid diagnosis of patients with LOC, both conveniently and objectively, while overcoming the limitations of the visual interpretation of EEG.

Although a common final pathophysiology of LOC is shared, several lines of evidence indicate that there are different intermediate mechanisms depending on the cause of LOC (Posner et al., 2019). Specifically, LOC due to ME or drug intoxication are not derived from abnormalities localized to a specific brain area, but because the overall function of the ascending reticular activating system (ARAS) is simultaneously impaired (Posner et al., 2019). In contrast, LOC due to focal-onset NCSE occurs when abnormal epileptic discharges originating from single or multifocal areas are synchronized, resulting in abnormalities throughout the functional network (van Diessen et al., 2013). Given the presence of focality, the properties of the functional network in focal-onset NCSE may be different from those in ME and BI (Kim et al., 2023). Moreover, because ME and BI may have different chemical substrates and neurotransmitters affecting brain function, the patterns of functional connectivity (FC) alteration implicated in the underlying mechanisms of LOC may differ between the two conditions.

Given these distinct mechanisms, we hypothesized that machine learning (ML) and deep learning (DL) models, trained on EEG FC data, can accurately differentiate the leading causes of LOC. Herein, we compared the EEG FC properties of focal-onset NCSE, ME, and BI. In addition, using the differences in network properties among the groups, we sought to evaluate the applicability of the FC-based ML and DL models for the differential diagnosis of LOC. Three modeling approaches were used: (1) a DL model utilizing convolutional neural network (CNN) with FC adjacency matrices, (2) ML algorithms with vectorized FC values, and (3) ML algorithms with graph theoretical measurements (GMs) as features. The DL model with CNN was chosen for its ability to capture complex spatial patterns in the FC adjacency matrices, which are crucial for identifying intricate brain connectivity patterns. The ML algorithms with vectorized FC values were selected because vectorization simplifies the data structure, making it suitable for traditional ML techniques and ensuring a broad application of various algorithms. Lastly, ML algorithms with GMs as features were incorporated to utilize the rich information provided by graph theory in characterizing network properties, thus enhancing the detection of subtle topological changes in brain networks. Each approach was methodically selected to complement the others and provide a comprehensive analysis of the data. To validate the reproducibility and clinical usability of the artificial intelligence (AI) model, we prospectively evaluated the performance of the FC-based ML and DL models in newly diagnosed patients with LOC. The study also applied explainable artificial intelligence (XAI) techniques to identify clinically relevant features related to LOC pathology. A schematic overview of the analytical process is shown in Fig. 1.

The present study is organized as follows. Section 2 describes the materials and methods used in the study, including subject selection, EEG recording, FC and graph theoretical analyses, AI modeling framework, and statistical analysis. Section 3 presents the results of the analyses, including feature extraction, performance of the AI-driven LOC classification models, and prospective validation. Section 4 discusses the findings, highlighting the implications of the results, limitations of the study, and potential future directions. Finally, Section 5 provides a summary of the main contributions and the significance of our findings.

1.1. Related work

The integration of ML and DL methodologies has notably advanced the field of EEG-based diagnostics. Numerous studies have utilized FC metrics derived from EEG data to classify consciousness states and predict outcomes in patients with disorders of consciousness and various neurological disorders. Research has demonstrated the efficacy of low-density EEG-based FC in distinguishing between minimally conscious state plus and minus, with ML techniques enhancing diagnostic precision (Secci et al., 2024). Further studies have utilized EEG-based connectivity features and CNNs to achieve a more nuanced understanding of consciousness states (Cai et al., 2024). Additionally, the correlation between EEG data and schizophrenia symptoms has been explored using both ML and DL across diverse data modalities, highlighting the potential of these techniques in various clinical conditions (Alves et al., 2023).

Despite these advancements, several gaps persist. For example, the prediction of residual consciousness in ICU patients using multimodal FC measures did not include the integration of XAI techniques to interpret model decisions (Amiri et al., 2023). Furthermore, various studies have applied EEG features and ensemble models like XGBoost for predicting recovery prognosis and detecting disorders of consciousness, but did not address the interpretability of these models (Ballanti et al., 2022; Wang et al., 2022).

Contributions of our study were to bridge these gaps by implementing a comprehensive approach that combines advanced feature extraction methods, diverse epoch sizes, and XAI techniques. (1) We employed three distinct feature extraction methods: three-dimensional FC adjacency matrices, vectorized FC values, and GMs, to construct robust classification models. This approach captures complex interactions within brain networks beyond simple comparisons or representation through single FC metrics. (2) By varying epoch sizes, we propose a framework to ensure the accuracy and practical utility of our classification models, determining the minimum data required for reliable performance. Multiple AI models were evaluated, including CNNs with 3D FC adjacency matrices, vectorized FC values, GM, and a combination of 3D FC adjacency matrices and GM. (3) To enhance the transparency and clinical applicability of our models, XAI techniques were incorporated to provide insights into the AI models' decision-making processes, thereby making the results more interpretable for clinical use. (4) Finally, our models were validated using a prospective validation cohort, demonstrating their robustness and reliability in real-world clinical settings, beyond traditional cross-validation methods. In summary, this study builds on the existing body of research by addressing key gaps in feature extraction, model interpretability, and validation, advancing the field of EEG-based diagnostics and offering novel insights for clinical applications.

2. Materials and methods

2.1. Subjects

This study was based on a retrospective review of an inpatient long-term video-EEG monitoring database between January 2019 and December 2020. From the entire database, we selected EEG data from patients confirmed to have focal-onset NCSE, ME, and BI through a comprehensive evaluation, including electroclinical diagnosis by board-certified epileptologists (HK and JBK), neuroimaging studies, and laboratory examinations. The inclusion criteria for focal-onset NCSE were as follows: (1) proven seizure onset focus, (2) EEG findings according to the Salzburg criteria for NCSE (Leitinger et al., 2016); and (3) recovery of consciousness after ASM treatment. The inclusion criteria for ME were as follows: (1) decreased consciousness associated with metabolic abnormalities documented by laboratory examinations, such as elevated liver enzymes, elevated creatinine and blood urea nitrogen levels, electrolyte imbalance, glucose abnormality, and septicemia; (2) recovery of consciousness after improvement of medical derangement without the use of ASMs or drugs that act directly on the central nervous system; (3) EEG findings that do not meet the Salzburg criteria for NCSE (Leitinger et al., 2016); and (4) absence of underlying epilepsy. The inclusion criteria for BI as follows: (1) proven history of taking

benzodiazepine; (2) only patients with LOC that had a close temporal relationship with the administration of benzodiazepine; (3) EEG findings that do not meet the Salzburg criteria for NCSE (Leitinger et al., 2016); (4) recovery of consciousness level after cessation of benzodiazepine or administration of flumazenil (Zamani et al., 2022) without use of ASMs or drugs that act directly on the central nervous system; and (5) who met the criteria for the "certain" and "probable" classifications of the World Health Organization-Uppsala Monitoring Centre (WHO-UMC) causality categories (Edwards and Aronson, 2000). For prospective validation, EEG data of patients with focal-onset NCSE, ME, and BI between January 2021 and December 2021 were included. The study followed the ethical guidelines of the Declaration of Helsinki and was approved by the Institutional Review Board of Korea University Anam Hospital (No. 2020AN0435).

2.2. Demographics

To avoid imbalanced sample sizes, 150 patients (50 in each group) were included in the analysis. The mean age ± SD for patients with NCSE, ME, and BI was 73.12 ± 12.86, 72.82 ± 13.39, and 60.64 ± 15.94 years, respectively. The proportions of women were 36 (72.0 %), 33 (66 %), and 33 (66 %) in the NCSE, ME, and BI groups, respectively.

2.3. EEG recording and epoch selection

EEG recordings were performed using a 32-channel recording system (Comet-PLUS; Grass Technologies Inc., West Warwick, RI, USA), and 19 channels were used with electrode placement according to the international 10s20 system (Klem et al., 1999), which is most commonly used in clinical practice, to achieve the purpose of this study in maximizing the utility value of the implemented AI models. The EEG data were sampled at 200 Hz, and the bandpass filter was set between 0.1 Hz and 70 Hz. This filter range is in accordance with guidelines from the International Federation of Clinical Neurophysiology (IFCN) and is widely used in clinical practice, as it helps to capture both slow-wave activities (e.g., delta waves) and high-frequency components (e.g., beta and gamma waves), while preventing baseline distortion and reducing high-frequency noise and artifacts, thereby improving the signal-to-noise ratio for accurate clinical interpretation (Nuwer et al., 1998). Consecutive 5-s, 10-s, 20-s, and 30-s epochs during LOC were carefully reviewed and selected by two board-certified epileptologists (HK and JBK) for each EEG dataset. Each epoch length was used for separate analyses. In this study, the analysis was centered around the 20-s epochs, with additional separate analyses conducted using 5-s, 10-s, and 30-s epochs to examine differences based on epoch size. To ensure the reliability of the analysis, EEG epochs were carefully selected that exhibited consistent pathological states without variability. The epoch selection criteria were as follows: (1) continuous presence of pathological EEG patterns indicative of the underlying LOC condition; (2) absence of artifacts, such as muscle movements, eye blinks, and electrode noise, to ensure data quality; (3) stability of the EEG signal, confirmed through visual inspection by experienced epileptologists, ensuring no transitions to different brain states; and (4) use of sufficiently long epochs (e.g., 1 min) to capture stable and representative EEG activity. To avoid arbitrariness in the choice of whether components are derived from brain signals or artifacts, and to maximize clinical utility by minimizing data processing costs, we did not apply any manipulations to remove artifacts or reduce noise through independent component analysis (ICA) or other automated methods.

2.4. Functional connectivity and graph theoretical analyses

The FC was evaluated using coherence, which reflects the level of functional signal communication between different regions of the brain (Thatcher et al., 1986). Coherence was selected as the FC measurement in this study because it is an undirected measure that accommodates individual variability in localized pathological regions and effectively captures pathophysiological differences across LOC causes through frequency domain analysis. Coherence is defined as follows:

$$COH_{xy} = k_{xy}{}^2(f) = |K_{xy}(f)|^2 = \frac{|S_{xy}(f)|^2}{S_{xx}(f)S_{yy}(f)} \quad (1)$$

where $S_{xy}(f)$ is the cross-spectral density between x and y, and $S_{xx}(f)$ and $S_{yy}(f)$ are the autospectral densities of x and y, respectively. where K is the coherency function. where $|S|$ denotes the modulus of S. The coherence value ranged between 0 and 1, with 0 denoting no statistical relationship and 1 denoting full coherence (Thatcher et al., 1986). The epochs were then bandpass filtered into the following frequency bands: delta (0.5–4 Hz), theta (4–8 Hz), alpha (8–13 Hz), beta (13–30 Hz), and gamma (30–50 Hz). Subsequent analyses were performed separately for each band. Coherence analysis and visualization were performed using tailored Python scripts and the MNE-Python package (version 1.5.1) (Gramfort et al., 2013).

Selected thresholds in the strength of the network can significantly affect the results of graph theoretical analysis, potentially causing variability and bias. Therefore, a weighted undirected network model of graph-theoretical analysis was used to mitigate arbitrariness in this study (Rubinov and Sporns, 2010). Twelve GMs (average degree, average strength, radius, diameter, characteristic path length, global efficiency, local efficiency, clustering coefficient, transitivity, modularity, assortativity, and small-worldness) were computed using the Brain Connectivity Toolbox (http://www.brain-connectivity-toolbox.net) and BRAPH toolbox (http://braph.org) working on MATLAB R2022b (MathWorks, Natick, MA, USA) (Mijalkov et al., 2017; Rubinov and Sporns, 2010). GMs were compared between groups using nonparametric tests with 1000 permutations. Statistical significance was set at $P < 0.05$ and was corrected for multiple comparisons using the false discovery rate.

2.5. AI modeling framework

2.5.1. Data preparation

We systematically extracted three forms of FC data as features for each classification model using three approaches. First, FC data were stratified into five frequency bands and organized into 3D FC adjacency matrices (5 × 19 × 19). The 19 × 19 dimensions included all possible combinations of coherence among the 19 EEG channels. Second, all FC pairs of the combinations were vectorized into a tabular data format (1 × 855). Finally, the GMs were processed as tabular data (1 × 60). The three forms of the data representing the brain network properties along with the corresponding three-class labels (i.e., NCSE, ME, and BI) were utilized for the training and validating the classifier model. The 3D FC adjacency matrices were processed by a CNN and the vectorized tabular data (FCs and GMs) were employed as input for a variety of ML models.

2.5.2. Model selection

2.5.2.1. Deep learning models for adjacency matrix data. This approach utilizes a CNN model based on 3D FC adjacency matrices. This model was chosen because CNNs are particularly effective in capturing spatial hierarchies in multi-dimensional data (LeCun et al., 2015). The CNN's ability to automatically and adaptively learn spatial features through hierarchical representations makes it ideal for analyzing the complex structures present in 3D FC adjacency matrices, which are crucial for distinguishing between different causes of LOC.

The front structure of the model is mainly characterized by iterative layers of convolution and max pooling. This configuration is repeated in four stacked layers, followed by data processing in three fully connected layers. This sequence culminates in the final prediction stage, where the model produces three distinct probabilistic outputs corresponding to each class. Fig. 2 presents the details of the CNN model architecture.

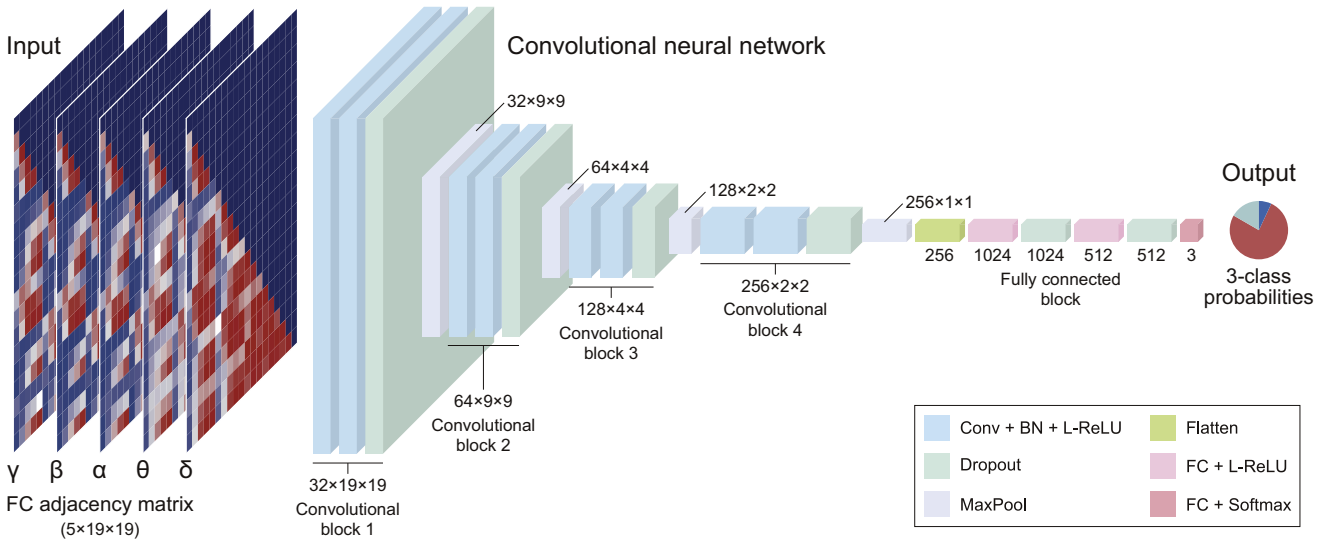

Fig. 2. Overview of the CNN model architecture. Conv = 2D convolutional layer (kernel: 3 × 3, padding: 1, stride: 1), MaxPool = 2D max pooling layer (kernel: 2 × 2, stride: 2), BN = batch normalization, L-ReLU = leaky rectified linear unit as an activation function, Dropout = dropout layer (dropout rate: 10 %), FC = fully connected layer.

Moreover, the classification performance of the LOC causes using a multi-domain CNN architecture that integrates both FC and GM information (Phang et al., 2019) was investigated. The pathway for processing the 3D FC adjacency matrices employs the same convolutional layers as the previously mentioned CNN model. For processing GM data, 12 GM data were stratified into five frequency bands (i.e., delta, theta, alpha, beta, gamma), resulting in 5 × 12 inputs. GM data with 5 × 12 format then is processed via 1D convolutional layers to efficiently capture patterns within the graph metrics. The two pathways are integrated into a single fully connected layer. Detailed information regarding this model architecture is provided in Suppl. Fig. 1.

2.5.2.2. Machine learning models for vectorized tabular data. The model embraces universally employed regular ML models, such as logistic regression, naïve Bayes, decision tree, random forest, support vector machine, and neural networks. These models were chosen to cover a wide range of learning paradigms, each with unique strengths. Logistic regression and naïve Bayes offer simplicity and interpretability for linearly separable data (Hosmer Jr et al., 2013). Decision trees and random forests are robust in handling non-linear relationships and interactions between features (Breiman, 2001). Support vector machines excel in high-dimensional spaces with clear margins between classes (Cortes and Vapnik, 1995). Neural networks provide flexibility in modeling complex, non-linear patterns (LeCun et al., 2015).

2.5.3. Parameter tuning

2.5.3.1. Deep learning models for adjacency matrix data. The training settings included the use of the cross-entropy loss as the criterion. The Adam optimizer was used for optimization and the learning rate is set to 0.001. The layer parameters included a kernel size of 3, stride of 1, and padding of 1 in convolutional blocks. A leaky rectified linear unit was employed as the activation function. To mitigate overfitting, we employed techniques such as regularization and dropout. Specifically, L2 regularization is applied with a weight decay of 10^{-6}, and a dropout rate of 0.1 is used in the model. These methods help prevent the model from becoming too complex and ensure better generalization to new data.

Model training was conducted over a maximum of 1000 epochs with the batch size set to 256, ensuring that all data points in the training set could fit into a single batch to utilize the benefits of batch processing and stabilizing gradient updates. The best model was selected based on the highest validation accuracy achieved during the training phase. The training and cross-validation processes were performed on a workstation equipped with an NVIDIA GeForce RTX 4070 GPU, supported by a 13th Generation Intel® Core™ i9–13900H CPU.

2.5.3.2. Machine learning models for vectorized tabular data. Based on the F-values, the input features were selected from all possible vectorized FC and GM features. Our approach involved prioritizing features with the highest F-values, gradually adding them one by one in order of significance. We monitored the performance on the test set with each addition to determine the optimal number of features. For every possible number of input features, we conducted a comprehensive grid search on the hyperparameters during the cross-validation process across six different ML models. The optimal combinations of input features and hyperparameters are summarized in Suppl. Table 1.

2.5.4. Model validation

To comprehensively evaluate the validity of the model and minimize overfitting, we utilized class-balanced 10-fold cross-validation using random sampling (Suppl. Fig. 2A). The retrospective dataset was divided into ten folds. Each iteration used one-fold for testing and the remaining nine folds for training, ensuring each fold served as the test set once. The rationale for choosing 10 folds is based on the balance it offers between bias and variance. Using 10 folds helps ensure that each subset is large enough to provide a reliable estimate of model performance while maintaining a manageable number of training and validation cycles. This method is widely accepted as providing a good trade-off between computational efficiency and robust estimation of the model's generalization capabilities (Refaeilzadeh et al., 2009). The true labels and predicted labels from all ten test sets were aggregated. By combining the results from all folds, we obtained a robust and representative assessment of the model's performance, avoiding biases that might arise from a single train-test split. For each patient, the predicted class was determined based on the highest probability among the three classes using softmax, and the three-class confusion matrix was derived from this. The performance of each model was evaluated using a confusion matrix containing the parameters of recall, precision, F1-score, and accuracy (Suppl. Fig. 2B). The receiver operating characteristic (ROC) curve and area under the ROC curve (AUC) was also calculated.

2.6. Explainable artificial intelligence

After obtaining the model outputs, a saliency map was computed to provide information regarding the contributions of individual FC values. The saliency map, which reflected the gradient magnitude of the FC values, was generated by applying backpropagation from the last classification layer of the model (Simonyan et al., 2013). The average saliency map across all cross validations takes the following form:

$$S_{c,\ total} = \frac{1}{K}\sum_{k=1}^{K} S_{c,\ k} \tag{2}$$

where $S_{c,\ total}$ denotes the mean saliency map for class c over k-fold cross-validation.

Shapley additive explanations (SHAP) values were used for XAI in the ML models (Lundberg et al., 2020). To obtain a comprehensive understanding of feature importance, this method entails assembling the SHAP values from all data points across each fold and finding the average of their absolute values to calculate the overall feature importance. The feature importance employed for this averaging process was as follows:

$$\text{Feature importance} = \frac{1}{K}\sum_{k=1}^{K}\frac{1}{n_k}\sum_{i=1}^{n_k}\left|\text{SHAP}_{i,k}\right| \tag{3}$$

where the SHAP value $\text{SHAP}_{i,k}$ is calculated for each feature i in each fold k using the formula, n_k is the number of samples in the kth fold, and K is the total number of folds. A SHAP summary plot was generated to depict the overall importance of each feature and how it influenced the model's predictions in terms of direction and magnitude. All development and evaluation processes related to ML and DL were conducted using PyTorch version 2.0.1, Scikit-learn version 1.3.1, and SHAP version 0.42.1, within Python version 3.9.0.

2.7. Prospective validation

Each model underwent a retraining phase on the entire retrospective dataset utilizing the optimal configurations identified from the 10-fold cross-validation procedure. For the CNN, 100 additional epochs were retrained using a retrospective dataset. The prospective dataset was evaluated once for each final model using three approaches. Overview of the validation procedure is presented in Suppl. Fig. 2A.

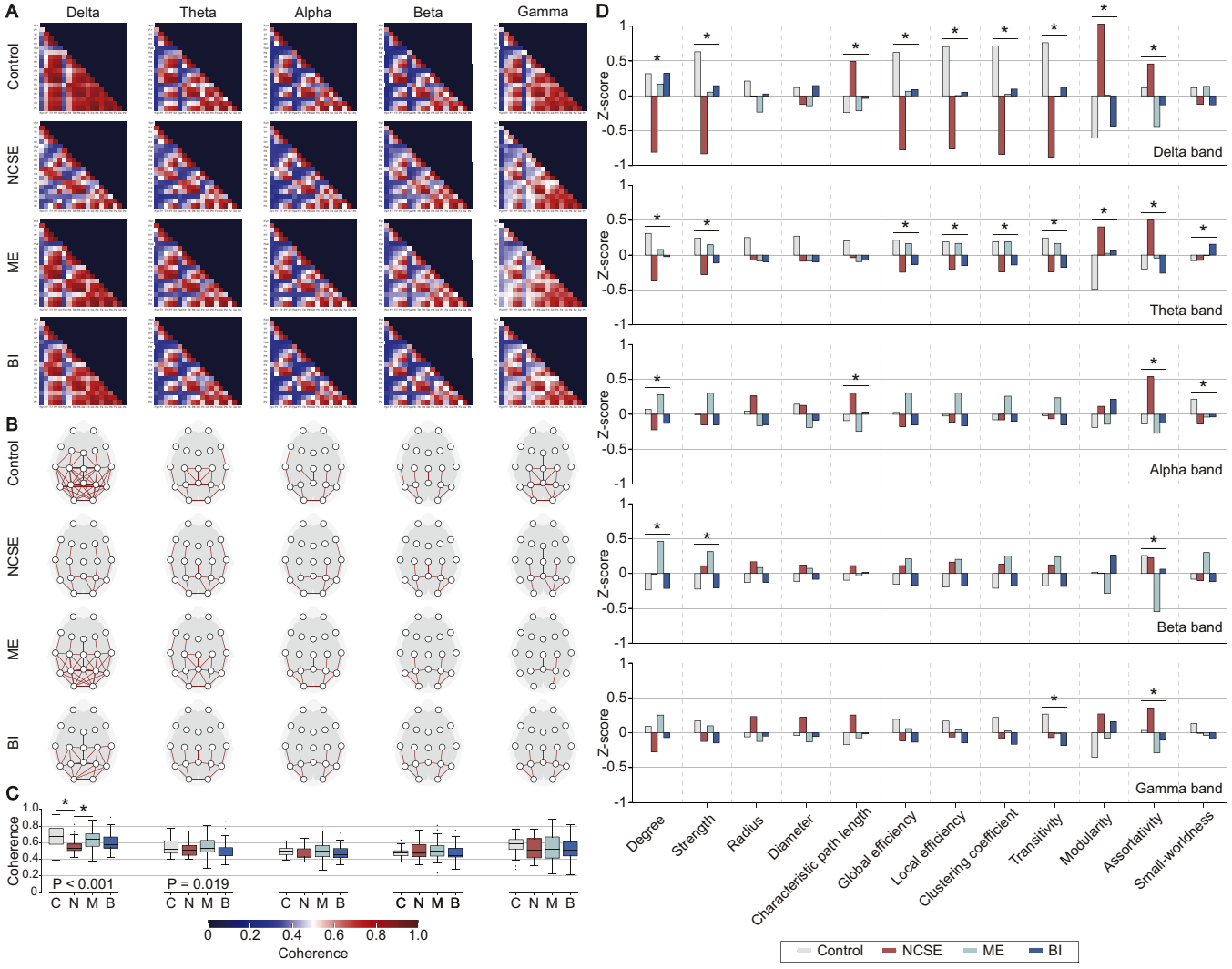

Fig. 3. FC measured by coherence values. (**A**) Coherence matrices. (**B**) Connections showing a coherence value of 0.80 or higher on a schematic model of EEG electrode locations according to the international 10–20 system. (**C**) Comparisons of averaged coherence values among the groups. The *P* values indicated below the box plots represent the statistical significance of the Kruskal-Wallis *H* test. Asterisks denote Bonferroni-corrected statistical significance by Mann-Whitney *U* test ($P < 0.0083$). (**D**) Comparisons of GM between the groups. Asterisks denote statistical significance by Kruskal-Wallis *H* test ($P < 0.05$). C: healthy control; N: NCSE; M: ME; B: BI.

2.8. Statistical analysis

To address the nonparametric characteristics and small sample sizes of the cohorts, the Kruskal-Wallis *H* test was employed for comparison among the four groups (NCSE, ME, BI, and healthy control). If the Kruskal-Wallis *H* test indicated significant differences, further pairwise comparisons between groups were conducted using the Mann-Whitney *U* test. The Bonferroni correction was applied to the p-values from these pairwise comparisons to account for multiple testing, adjusting the significance level to reduce the likelihood of Type I errors. With six pairwise comparisons, the Bonferroni-adjusted significance threshold was set at $P < 0.0083$ (0.05/6). Statistical significance was originally set at $P < 0.05$. In addition to statistical significance, effect sizes were calculated to quantify the magnitude of differences. For the Kruskal-Wallis H-test, the eta-squared (η^2) effect size was computed to provide a measure of the variance explained by the group differences. For the Mann-Whitney *U* test, the Cliff's delta (δ) was calculated to assess the effect size for pairwise comparisons. All statistical analyses were performed using SciPy version 1.10.1.

3. Results

3.1. Feature extraction: functional connectivity and graph theoretical analyses

The FC patterns of the healthy control (HC) and LOC patient groups are presented in Fig. 3A-C. Compared to the HC group, the FC of the LOC group was found to have decreased density in the posterior regions. The reduced FC density was most pronounced in the NCSE group ($P < 0.001$, $\eta^2 = 0.161$), especially in the delta band. FC differences between all groups were found in the theta band ($P = 0.019$, $\eta^2 = 0.036$), whereas no differences were observed in multiple comparisons between individual groups. Comparisons of FC between the HC and merged LOC groups are shown in the Suppl. Fig. 3.

Between-group comparisons of the GM standardized by z-scores are shown in Fig 3D. Differences in the GM between the LOC groups were most pronounced in the delta band. In addition, there were differences in assortativity between the groups, with NCSE being higher than the other LOC groups in all frequency bands. The between-group comparisons of GM are detailed in the Suppl. Table 2.

Table 1
Performance of three approaches: DL model using FC adjacency matrix, ML with vectorized FC, and ML with GM.

Model	Accuracy	AUC	Recall	Precision	F1-score
FC adjacency matrix					
Convolutional Neural Network	0.880	0.905	0.880	0.890	0.881
Vectorized FC					
Logistic Regression	0.760	0.893	0.760	0.766	0.762
Naive Bayes	0.673	0.820	0.673	0.678	0.667
Decision Tree	0.727	0.774	0.727	0.727	0.723
Random Forest	0.753	0.881	0.753	0.751	0.752
Support Vector Machine	0.753	0.882	0.753	0.761	0.756
Neural Network	0.740	0.881	0.740	0.739	0.739
Vectorized GM					
Logistic Regression	0.693	0.831	0.693	0.691	0.692
Naive Bayes	0.567	0.768	0.567	0.555	0.543
Decision Tree	0.540	0.698	0.540	0.546	0.526
Random Forest	0.660	0.812	0.660	0.658	0.658
Support Vector Machine	0.667	0.812	0.667	0.665	0.665
Neural Network	0.640	0.813	0.640	0.640	0.636

3.2. Performance: AI-driven LOC classification models

The performance of the three AI approaches in the classification of LOC causes is presented in Table 1 and detailed in the Suppl. Table 3. The DL model (i.e., the CNN model based on FC adjacency matrices) attained the highest overall accuracy, with an AUC of 0.905. Among the three classes, NCSE classification using the DL model achieved the highest accuracy, with an AUC of 0.938 (Suppl. Table 3). Among the six applied ML models, logistic regression (LR) showed the highest accuracy when both vectorized FC and GM were used as features, achieving AUCs values of 0.893 and 0.831, respectively. Details on the performance of AI models according to the epoch size are presented in Suppl. Fig. 4. The accuracy increased to 20-s epoch, and the performance converged when the size increased to 30-s epoch. The performance of the multi-domain CNN model was higher than that of models using FC adjacency matrices alone for 5-s and 10-s epochs, while it was lower for 20-s and 30-s epochs.

The detailed performance metrics of the models showing the best performance for each approach are shown in Fig 4. The CNN model exhibited superior classification performance compared with the ML models, with pronounced true positive rates, as shown by its ROC curve (AUC = 0.905) and confusion matrix (classification accuracy = 0.880; Fig 4A). The prediction probabilities of each classification model at the individual subject level are presented in the right panel of Fig 4. The LR model was the most accurate among the ML models based on both vectorized FC and GM, and NCSE was classified with higher accuracy than ME and BI.

3.3. XAI: Interpreting functional connectivity signatures

Saliency maps visualizing the features on which the CNN model focused in each LOC group are shown in Fig 5. The most salient features of the LOC classification were found in the theta and delta bands. Features of the FC adjacency matrices in the theta band were focused on classifying NCSE, whereas those in the delta band were focused on classifying BI.

Suppl. Fig. 5 shows the SHAP importance matrix plots, which depict the power and classification direction of the top 20 most contributing FC features to the LR, which achieved the highest accuracy among the applied ML models. In all three LOC groups, the FC values found to be the top 20 most important features were exclusively in the delta and theta bands.

An interpretation of the GM-based LR model is presented in Suppl. Fig. 6. Transitivity, modularity, strength, and degree in the delta band were important features of the classification model. In addition, the assortativity in the delta, alpha, and beta bands was identified as an important feature of the model.

3.4. Prospective validation

AI models with the three approaches implemented using preexisting databases were prospectively validated by applying them to a new dataset from the LOC cohort. The detailed validation results are shown in Fig. 6. The FC adjacency matrix-based CNN model retained high performance in classifying NCSE, ME, and BI, with AUCs of 0.830, 0.860, and 0.965, respectively (Fig. 6A). The validation performances of the ML models using the vectorized FC (Fig. 6B) and GM (Fig. 6C) features were inferior to that of the CNN model. The detailed performance metrics are presented in the Suppl. Table 4.

4. Discussion

In this study, we explored FC properties among focal-onset NCSE, ME, and BI. We employed FC-based ML and DL models to differentiate the three groups. The major findings of this study are as follows: (1) Compared to controls, the overall FC density in the delta band was lower

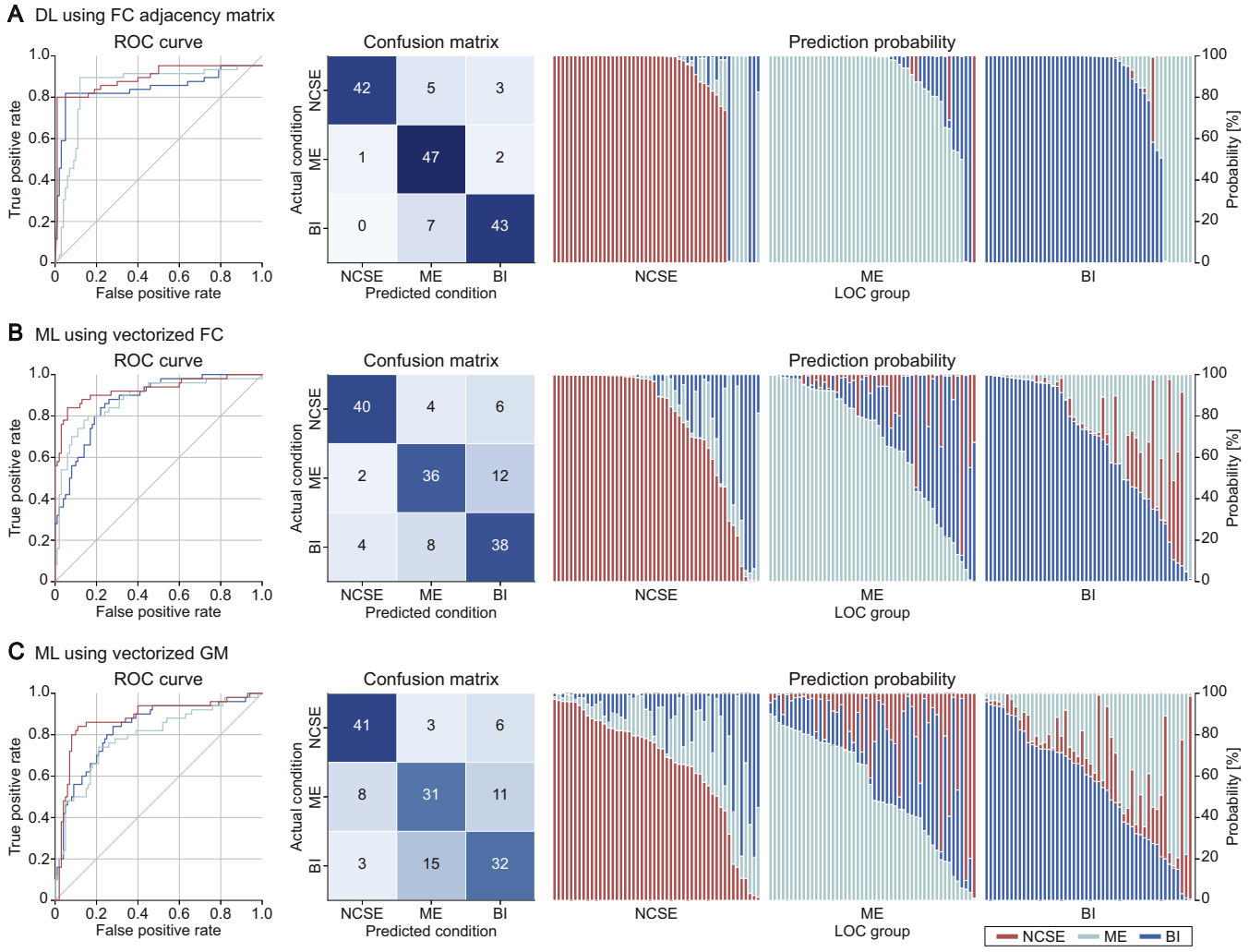

Fig. 4. Performances of the three optimal AI models. ROC curves (left panel) and confusion matrices (middle panel) for the classification performance of the most accurate model in each approach. Bar plots (right panel) illustrate prediction probabilities of the model in the level of individual subjects: (**A**) FC adjacency matrix-based DL model (CNN). (**B**) ML model using vectorized coherence (LR). (**C**) GM-based ML model (LR).

in LOC groups, especially in parieto-centro-frontal connections. Graph analysis indicated network disintegration in LOC patients. Differences in network characteristics were primarily in the delta and theta bands; (2) FC and GM exhibited unique patterns within each LOC group, predominantly in the delta and theta bands; (3) AI models using network features as inputs demonstrated high accuracy, with the FC adjacency matrix-based CNN model achieving the best performance, showing a multi-class classification AUC above 0.900. NCSE was most accurately classified across all models; (4) XAI models revealed that AI models focused on delta and theta band features for LOC classification; (5) Using prospective cohort data, we confirmed the high accuracy and reproducibility of our AI models.

The human brain is complex. In addition, the brain does not rely on the activity of an individual region to function but rather physiologically requires FC between multiple spatially separated regions (Bullmore and Sporns, 2009; Power et al., 2011). From a network perspective, for consciousness to be preserved, the FC in the ARAS encompassing the brainstem and diencephalon, including the thalamus, basal forebrain, and cerebral cortex, should be normal (Moruzzi and Magoun, 1949). Therefore, approaches to FC and complex network analyses, rather than investigations of neural activities in a single region, may be appropriate for quantitative assessments of consciousness levels and differential diagnosis of the cause of LOC. We identified a reduction in FC density in patients with LOC compared to controls, with a particularly pronounced disconnection in the parietofrontal regions corresponding to the thalamocortical circuit. Several lines of evidence indicate that altered modulations in the thalamus and thalamocortical circuits may be implicated in the fundamental pathophysiological mechanisms underlying impaired consciousness (Cauda et al., 2009; Crone et al., 2015, 2014; Laureys et al., 2000; Laureys and Schiff, 2012; Vanhaudenhuyse et al., 2010; Zhou et al., 2011). In addition, cortico-thalamo-cortical (CTC) loops can influence corticocortical connectivity through the modulation of excitatory and inhibitory signals by γ-aminobutyric acid (GABA)ergic neurons embedded throughout the CTC loops (Sanchez-Vives et al., 2021; Shepherd and Yamawaki, 2021). Based on the above-mentioned knowledge, we speculate that our findings of reduced FC density in the parietofrontal regions in the LOC group could be interpreted as disrupted corticocortical FC caused by impairments in the CTC loops or CTC-corticocortical loop chains. Given that the thalamus acts as a generator of delta oscillation (Rivera-Lillo et al., 2021; Schanze and Eckhorn, 1997), our finding that FC abnormalities in the LOC are more pronounced in the delta band further supports our speculation. In addition, considering the pivotal role of the thalamocortical circuit in the default mode network (Fernandez-Espejo et al., 2012) and ARAS (Moruzzi and Magoun, 1949), our findings are consistent with the well-known notion that thalamocortical disconnection is implicated in the common pathophysiology underlying LOC.

Graph theoretical analysis showed that LOC patients had networks

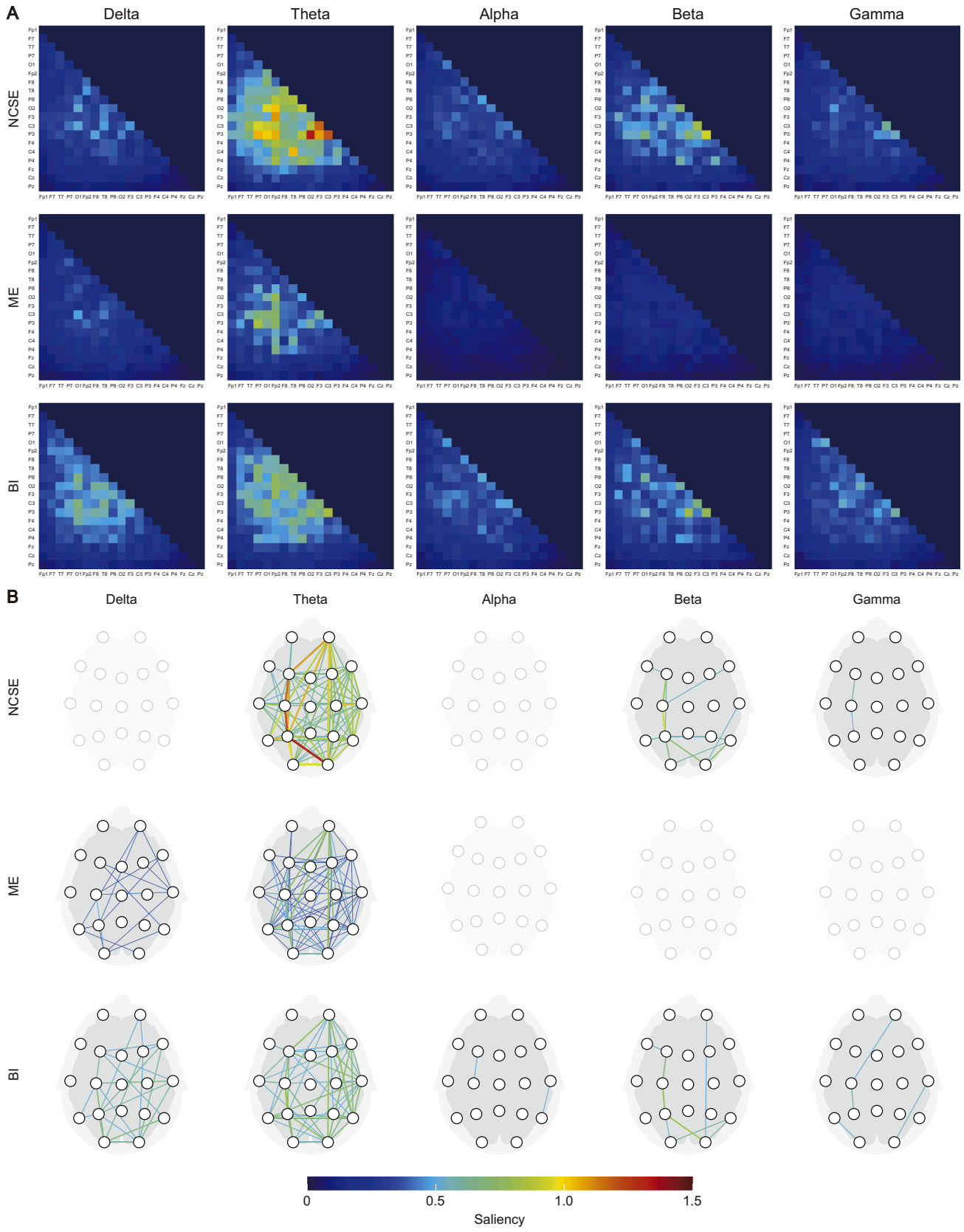

Fig. 5. DL model interpretation through 3D FC adjacency matrix saliency mapping. (**A**) Group-specific saliency value distribution matrix. (**B**) Visualization of the highest 10 % of saliency values of FC features registered on the EEG electrode locations based on the international 10–20 system. Transparent maps indicate that no saliency values were selected in the XAI model.

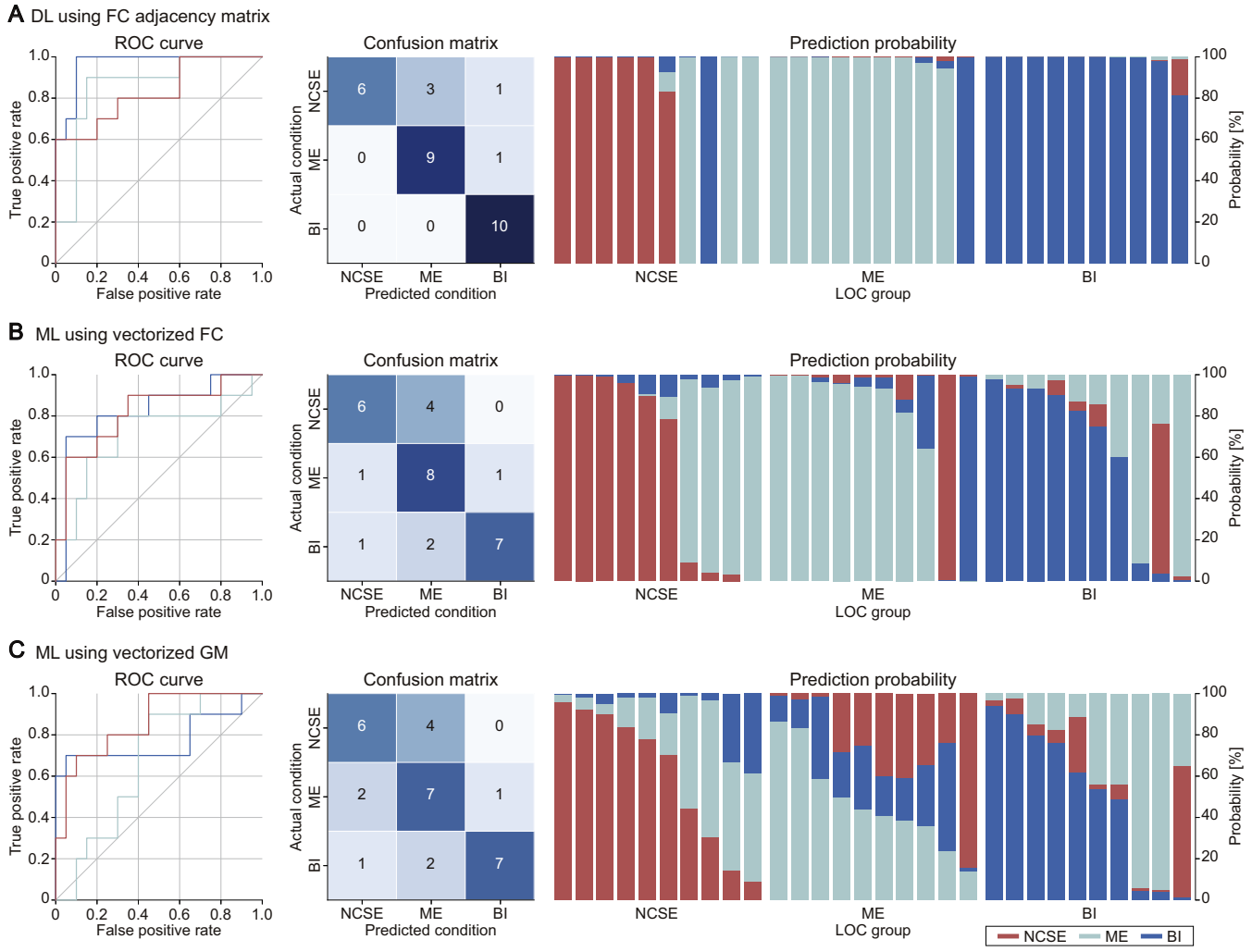

Fig. 6. Prospective validation of the three AI models. ROC curves (left panel) and confusion matrices (middle panel) for the classification performance of the most accurate model in each approach. Bar plots (right panel) illustrate prediction probabilities of the model in the level of individual subjects: (**A**) FC adjacency matrix-based DL model (CNN). (**B**) ML model using vectorized coherence (LR). (**C**) GM-based ML model (LR).

characterized by reduced integration (Bullmore and Sporns, 2009). Consciousness can be maintained normally when the organic integration across the consciousness-related brain regions is preserved, whereas the level of consciousness can be impaired when the integration is impaired and becomes segregated (Panda et al., 2023). Previous studies using graph theoretical analysis have demonstrated the loss of network integrity in LOC (Panda et al., 2023; Tan et al., 2019; Yang et al., 2023, 2018), and the reorganization of the network between the components within the ARAS may be the fundamental in the pathophysiological mechanism underlying LOC in terms of large-scale complex networks. Taken together, the FC and GM characteristics found in our population are in line with previous knowledge that impaired thalamocortical connectivity plays a pivotal role in the development of LOC.

Distinct patterns were observed in FC and GM in each of the three LOC groups. A significant difference was found in the overall FC strength in the delta band (Fig. 2), with the NCSE group having a lower strength than the ME group. In addition, NCSE was characterized by a more disintegrated network than the other two LOC groups. The pathophysiology of ME is understood to involve neurotoxicity from medical derangement asssffecting the entire brain, leading to lower GABA type B ($GABA_B$) receptor density and reduced feedback inhibition of $GABA_B$ on $GABA_A$ activity, resulting in the impairments of consciousness (Basile and Jones, 1997). BI can develop by direct inhibition of $GABA_A$ receptors distributed throughout the brain (Posner et al., 2019), which suppresses the entire central nervous system, including the ARAS and limbic system (Sanchez-Vives et al., 2021). Although ME and BI have different mediating processes at the $GABA_A$ and $GABA_B$ receptors as intermediary mechanisms, they affect the entire brain, resulting in a uniform distribution of FC damage and a relatively preserved integrity of the properties of large-scale complex networks. On the other hand, the altered network in focal-onset NCSE originates from a focal abnormality (Cui et al., 2020; van Diessen et al., 2013), and thus, the global network properties of focal-onset NCSE could be more segregated than those of ME or BI (Kim et al., 2023). The assortativity value, an indicator reflecting the resilience of the network (Newman, 2002), was observed to be higher in all frequency bands in the NCSE group than in the other groups, which could be interpreted as a result of the localized nature of the pathophysiological mechanisms of NCSE and the tendency to preserve the resilience of the network in areas where function is normally preserved.

There is an ongoing unmet need for quantitative markers for the differential diagnosis of LOC because EEG is often difficult to perform, and even when performed, cause-specific patterns are difficult to detect by visual interpretation. We found that the FC and GM for each LOC group exhibited distinctive patterns, and that the group-specific network patterns were relevant to the pathophysiological mechanisms of each etiology. Moreover, the functional network-based AI models achieved high performance, with AUC values exceeding 0.900. The high accuracy

of the differential diagnosis models might be attributed to the network properties used as features reflecting the pathophysiological mechanisms characteristic of each cause of LOC. Among the three approaches applied in this study, the CNN DL model showed the highest accuracy. It is plausible that the FC adjacency matrices from all frequency bands and features in the CNN DL model may comprehensively reflect all FC characteristics at once without loss of information, which could be the most optimal feature for the classification models. In addition, a graph is an abstract representation of a network, and each graph's theoretical measurement can only quantify the characteristics of a network from the perspective of the corresponding measures (Stam and Reijneveld, 2007). Therefore, we speculate that there may be considerable information loss when integrating the characteristics of the network using the GM, resulting in a lower classification accuracy of the ML model using the GM than that of other models. Our findings that the integrated model using 3D FC adjacency matrices and GM as features did not show higher accuracy compared to the model using only 3D FC adjacency matrices support our hypothesis. Considering the computational costs required for the integrated model, the CNN using only FC adjacency matrices with 20-s epoch EEG data can be considered the most efficient and optimal model. When applying AI models to the three LOC groups, the NCSE group was classified with the highest classification accuracy of 94.0 % in the CNN DL model. This finding might be partly explained by differences in the distribution of the pathophysiology involved in LOC (i.e., widespread in ME and BI vs. localized to the epileptogenic zone in NCSE).

Through application of the XAI techniques, we found that the AI models mainly focused on the differences in group-specific features in the delta band during classification. Considering that the thalamus and thalamocortical circuits are the main generators of delta band oscillations, the results of the XAI models may be in line with the previous knowledge that alterations in thalamocortical connectivity are fundamental mechanisms of LOC. Our classification models are believed to have classified the causes of LOC with high accuracy and biological and pathophysiological relevance and once again emphasize that FC and network analyses can be optimal frameworks for the differential diagnosis of patients with LOC.

Several limitations of this study should be considered when interpreting its results. First, the sample size is relatively small. Although the sample size to ensure the robustness and generalizability of the results of AI-driven analysis is unclear, one study found evidence for the diagnosis and prediction of LOC prognosis from studies involving more than 50 patients (Noirhomme et al., 2017). Given that our findings were derived from a sample of 150 patients (50 in each LOC group), we believe that they were not affected by overfitting. Second, we analyzed the FC at the sensor level using scalp EEG. Because of the lack of information at the source level, the data could inevitably be affected by volume conduction effects; thus, the exact anatomical localization of the generator of specific frequency oscillations and that of the local network was limited to speculation. Third, our study used a limited number of EEG channels at specific locations, which may affect generalization to other datasets with different channel configurations. To address this limitation, future research needs to evaluate the performance of AI models with different numbers and configurations of EEG channels. External validation using larger and more diverse datasets is required to confirm the robustness and generalizability of our models. Finally, although the XAI models have consistently paid attention to FC patterns in the low-frequency bands (i.e., delta and theta bands), important features were found to be different in detail according to the models and the domains of used features. Further studies should be required to reveal the most optimal approach for enhancing interpretability and clinical applicability.

Ethical implications of using AI models in clinical settings, focusing on patient data privacy and the potential consequences of misdiagnosis, should be considered. We believe the risk of personal information leakage is minimal because we used an AI model based solely on EEG data without any clinical information about the patient. In addition, since quantitative EEG metrics are processed measures of FC rather than raw biosignal data, it is nearly impossible to identify individuals. Moreover, the AI model is as small as 7.5 MB and can be processed within the device without external computing. Nevertheless, to evolve into cloud-based big data software medical devices and broader clinical diagnostic applications utilizing AI models in the future, it is essential to ensure data anonymization and address strict personal security concerns. Furthermore, to utilize AI models as diagnostic medical devices, it is important to develop final models with high accuracy, provide information on misdiagnosis rates, and establish clear regulatory guidelines on the clinical role and limitations of AI models.

Our study revealed that AI models, utilizing EEG FC matrices, can effectively differentiate between causes of LOC. In addition, we demonstrated that the accuracy of these classifications was reproducible through prospective validation. The AI model's performance shows a clear trend across different epoch sizes. Accuracy tends to increase as the epoch size grows from 5-s to 20-s, reaching its peak at the 20-s epoch. Beyond this point, the accuracy stabilizes, indicating that the epoch size to 30-s does not yield significant additional benefits (Suppl. Fig. 4A). These results suggest that the AI model can provide accurate LOC differentiation with a relatively small amount of EEG data in the 20-s, which may be clinically useful. To maximize clinical utility in real-time applications, further studies are required to determine whether high accuracy can be maintained with shorter data segments than the 20-s epoch data used in our study. Moreover, further studies should determine whether the performance of AI models with data from fewer than 19 EEG channels can still yield high accuracy. To ensure practical implementation in clinical settings, developing a software platform equipped with the developed AI algorithms is essential. This platform facilitates real-time application by processing EEG time-series data streams, significantly enhancing integration into clinical workflows. Furthermore, our findings, which highlight distinct network characteristics depending on the cause of LOC and incorporate these insights into AI models, could provide deeper understanding into the mechanisms underlying cause-specific functional networks.

There have been various studies applying AI using FC-based metrics for diagnosing and differentiating neurological disorders, including consciousness disorders (Adebisi et al., 2024; Phang et al., 2019; Yang et al., 2024). However, our study distinguishes itself by incorporating a comprehensive approach. It not only employs advanced feature extraction methods but also integrates a range of epoch sizes and XAI techniques, allowing for a more detailed capture of the complex interactions within brain networks. Additionally, we use multiple AI models, such as CNN with three-dimensional FC adjacency matrices and GMs, to ensure a robust and reliable classification. Furthermore, our prospective validation cohort demonstrates the real-world applicability of our models, enhancing their clinical relevance beyond traditional cross-validation methods. These contributions significantly advance the field of EEG-based diagnostics, addressing key gaps in feature extraction, model interpretability, and validation.

5. Conclusion

Our research uniquely applied network-related metrics from multiple perspectives and compared different epoch sizes to propose the optimal metric form, appropriate epoch size, and algorithm type. Notably, our study demonstrated high classification accuracy in multiclass classification, suggesting that FC-based AI models could serve as a valuable framework for diagnosis and differential diagnosis in neurological disorders where network abnormalities are central to pathophysiology.

CRediT authorship contribution statement

Young-Tak Kim: Writing – review & editing, Writing – original draft, Methodology, Investigation, Funding acquisition, Formal analysis. **Hayom Kim:** Writing – review & editing, Writing – original draft,

Methodology, Investigation, Formal analysis, Data curation, Conceptualization. **Mingyeong So:** Writing – review & editing, Investigation. **Jooheon Kong:** Writing – review & editing, Investigation. **Keun-Tae Kim:** Writing – review & editing, Investigation. **Je Hyeong Hong:** Writing – review & editing, Investigation. **Yunsik Son:** Writing – review & editing, Investigation. **Jason K. Sa:** Writing – review & editing, Investigation. **Synho Do:** Writing – review & editing, Investigation. **Jae-Ho Han:** Writing – review & editing, Investigation. **Jung Bin Kim:** Writing – review & editing, Writing – original draft, Methodology, Investigation, Funding acquisition, Formal analysis, Data curation, Conceptualization.

Declaration of competing interest

The authors declare no competing interests.

Data and code availability

The dataset used and analyzed during the current study is available from the corresponding author upon reasonable request. The underlying code for this study is available in GitHub repository and can be accessed via this link (https://github.com/KoreaUnivNeurology/LOC).

Acknowledgments

This work was supported by the Basic Science Research Program through the National Research Foundation of Korea (NRF), funded by the Ministry of Education (No. 2020R1I1A1A01073998, No. RS-2023-00212574). It was also supported by the Korea University College of Medicine (No. K2317041, No. K2325531), the Korea Medical Device Development Fund grant funded by the Korean government (Project Number: RS-2022-00140542), and a grant from the Korea Health Technology R&D Project through the Korea Health Industry Development Institute (KHIDI), funded by the Ministry of Health & Welfare, Republic of Korea (Grant Number: HI22C0946).

Supplementary materials

Supplementary material associated with this article can be found, in the online version, at doi:10.1016/j.neuroimage.2024.120749.

References

Adebisi, A.T., Lee, H.-W., Veluvolu, K.C., 2024. EEG-based brain functional network analysis for differential identification of dementia-related disorders and their onset. IEEE Trans. Neural Syst. Rehabil. Eng. 32, 1198–1209. https://doi.org/10.1109/TNSRE.2024.3374651.

Aguilon-Leiva, J.J., Tejada-Garrido, C.I., Echaniz-Serrano, E., Mir-Ramos, E., Torres-Perez, A.M., Lafuente-Jimenez, A., Martinez-Soriano, M., Santolalla-Arnedo, I., Czapla, M., Smereka, J., Juarez-Vela, R., Satustegui-Dorda, P.J., 2022. Clinical and sociodemographic profile of acute intoxications in an emergency department: a retrospective cross-sectional study. Front. Public Health 10, 990262. https://doi.org/10.3389/fpubh.2022.990262.

Alves, C.L., Toutain, T., Porto, J.A.M., Aguiar, P.M.C., de Sena, E.P., Rodrigues, F.A., Pineda, A.M., Thielemann, C., 2023. Analysis of functional connectivity using machine learning and deep learning in different data modalities from individuals with schizophrenia. J. Neural Eng. 20, 056025 https://doi.org/10.1088/1741-2552/acf734.

Amiri, M., Fisher, P.M., Raimondo, F., Sidaros, A., Cacic Hribljan, M., Othman, M.H., Zibrandtsen, I., Albrechtsen, S.S., Bergdal, O., Hansen, A.E., Hassager, C., Hojgaard, J.L.S., Jakobsen, E.W., Jensen, H.R., Moller, J., Nersesjan, V., Nikolic, M., Olsen, M.H., Sigurdsson, S.T., Sitt, J.D., Solling, C., Welling, K.L., Willumsen, L.M., Hauerberg, J., Larsen, V.A., Fabricius, M., Knudsen, G.M., Kjaergaard, J., Moller, K., Kondziella, D., 2023. Multimodal prediction of residual consciousness in the intensive care unit: the CONNECT-ME study. Brain 146, 50–64. https://doi.org/10.1093/brain/awac335.

Ballanti, S., Campagnini, S., Liuzzi, P., Hakiki, B., Scarpino, M., Macchi, C., Oddo, C.M., Carrozza, M.C., Grippo, A., Mannini, A., 2022. EEG-based methods for recovery prognosis of patients with disorders of consciousness: a systematic review. Clin. Neurophysiol. 144, 98–114. https://doi.org/10.1016/j.clinph.2022.09.017.

Basile, A.S., Jones, E.A., 1997. Ammonia and GABA-ergic neurotransmission: interrelated factors in the pathogenesis of hepatic encephalopathy. Hepatology 25, 1303–1305. https://doi.org/10.1002/hep.510250636.

Breiman, L., 2001. Random forests. Mach. Learn. 45, 5–32. https://doi.org/10.1023/A:1010933404324.

Bullmore, E., Sporns, O., 2009. Complex brain networks: graph theoretical analysis of structural and functional systems. Nat. Rev. Neurosci. 10, 186–198. https://doi.org/10.1038/nrn2575.

Cai, L., Wei, X., Qing, Y., Lu, M., Yi, G., Wang, J., Dong, Y., 2024. Assessment of impaired consciousness using EEG-based connectivity features and convolutional neural networks. Cogn. Neurodyn. 18, 919–930. https://doi.org/10.1007/s11571-023-09944-0.

Campbell, T.J., Men, S., Shearer, D., Ebejer, T., Joosse, M., Quercia, J., Sanders, J., Tadrous, M., Antoniou, T., Gomes, T., Ontario Drug Policy Research Network Citizens, P., 2023. The epidemiology of benzodiazepine-related toxicity in Ontario, Canada: a population-based descriptive study. Can. J. Public Health 1–11. https://doi.org/10.17269/s41997-023-00784-3.

Cauda, F., Micon, B.M., Sacco, K., Duca, S., D'Agata, F., Geminiani, G., Canavero, S., 2009. Disrupted intrinsic functional connectivity in the vegetative state. J. Neurol. Neurosurg. Psychiatr. 80, 429–431. https://doi.org/10.1136/jnnp.2007.142349.

Cortes, C., Vapnik, V., 1995. Support-vector networks. Mach. Learn. 20, 273–297. https://doi.org/10.1007/BF00994018.

Crone, J.S., Schurz, M., Holler, Y., Bergmann, J., Monti, M., Schmid, E., Trinka, E., Kronbichler, M., 2015. Impaired consciousness is linked to changes in effective connectivity of the posterior cingulate cortex within the default mode network. Neuroimage 110, 101–109. https://doi.org/10.1016/j.neuroimage.2015.01.037.

Crone, J.S., Soddu, A., Holler, Y., Vanhaudenhuyse, A., Schurz, M., Bergmann, J., Schmid, E., Trinka, E., Laureys, S., Kronbichler, M., 2014. Altered network properties of the fronto-parietal network and the thalamus in impaired consciousness. Neuroimage Clin. 4, 240–248. https://doi.org/10.1016/j.nicl.2013.12.005.

Cui, Y., Liu, J., Luo, Y., He, S., Xia, Y., Zhang, Y., Yao, D., Guo, D., 2020. Aberrant connectivity during pilocarpine-induced status epilepticus. Int. J. Neural Syst. 30, 1950029 https://doi.org/10.1142/S0129065719500291.

Edwards, I.R., Aronson, J.K., 2000. Adverse drug reactions: definitions, diagnosis, and management. Lancet 356, 1255–1259. https://doi.org/10.1016/S0140-6736(00)02799-9.

Fernandez-Espejo, D., Soddu, A., Cruse, D., Palacios, E.M., Junque, C., Vanhaudenhuyse, A., Rivas, E., Newcombe, V., Menon, D.K., Pickard, J.D., Laureys, S., Owen, A.M., 2012. A role for the default mode network in the bases of disorders of consciousness. Ann. Neurol. 72, 335–343. https://doi.org/10.1002/ana.23635.

Gramfort, A., Luessi, M., Larson, E., Engemann, D.A., Strohmeier, D., Brodbeck, C., Goj, R., Jas, M., Brooks, T., Parkkonen, L., Hamalainen, M., 2013. MEG and EEG data analysis with MNE-Python. Front. Neurosci. 7, 267. https://doi.org/10.3389/fnins.2013.00267.

Grant, A.C., Abdel-Baki, S.G., Weedon, J., Arnedo, V., Chari, G., Koziorynska, E., Lushbough, C., Maus, D., McSween, T., Mortati, K.A., Reznikov, A., Omurtag, A., 2014. EEG interpretation reliability and interpreter confidence: a large single-center study. Epilepsy Behav. 32, 102–107. https://doi.org/10.1016/j.yebeh.2014.01.011.

Hosmer Jr, D.W., Lemeshow, S., Sturdivant, R.X., 2013. Applied Logistic Regression. John Wiley & Sons, Hoboken. https://doi.org/10.1002/0471722146.

Kim, S.H., Kim, H., Kim, J.B., 2023. Differences in functional network between focal onset nonconvulsive status epilepticus and toxic metabolic encephalopathy: application to machine learning models for differential diagnosis. Cogn. Neurodyn. 17, 845–853. https://doi.org/10.1007/s11571-022-09877-0.

Klem, G.H., Luders, H.O., Jasper, H.H., Elger, C., 1999. The ten-twenty electrode system of the international federation. The international federation of clinical neurophysiology. Electroencephalogr. Clin. Neurophysiol. Suppl. 52, 3–6.

Laureys, S., Faymonville, M.E., Luxen, A., Lamy, M., Franck, G., Maquet, P., 2000. Restoration of thalamocortical connectivity after recovery from persistent vegetative state. Lancet 355, 1790–1791. https://doi.org/10.1016/s0140-6736(00)02271-6.

Laureys, S., Schiff, N.D., 2012. Coma and consciousness: paradigms (re)framed by neuroimaging. Neuroimage 61, 478–491. https://doi.org/10.1016/j.neuroimage.2011.12.041.

LeCun, Y., Bengio, Y., Hinton, G., 2015. Deep learning. Nature 521, 436–444. https://doi.org/10.1038/nature14539.

Leitinger, M., Trinka, E., Gardella, E., Rohracher, A., Kalss, G., Qerama, E., Hofler, J., Hess, A., Zimmermann, G., Kuchukhidze, G., Dobesberger, J., Langthaler, P.B., Beniczky, S., 2016. Diagnostic accuracy of the Salzburg EEG criteria for non-convulsive status epilepticus: a retrospective study. Lancet Neurol. 15, 1054–1062. https://doi.org/10.1016/S1474-4422(16)30137-5.

Lundberg, S.M., Erion, G., Chen, H., DeGrave, A., Prutkin, J.M., Nair, B., Katz, R., Himmelfarb, J., Bansal, N., Lee, S.I., 2020. From local explanations to global understanding with explainable AI for trees. Nat. Mach. Intell. 2, 56–67. https://doi.org/10.1038/s42256-019-0138-9.

Meierkord, H., Holtkamp, M., 2007. Non-convulsive status epilepticus in adults: clinical forms and treatment. Lancet Neurol. 6, 329–339. https://doi.org/10.1016/S1474-4422(07)70074-1.

Mijalkov, M., Kakaei, E., Pereira, J.B., Westman, E., Volpe, G., 2017. BRAPH: a graph theory software for the analysis of brain connectivity. PLoS ONE 12, e0178798. https://doi.org/10.1371/journal.pone.0178798.

Moruzzi, G., Magoun, H.W., 1949. Brain stem reticular formation and activation of the EEG. Electroencephalogr. Clin. Neurophysiol. 1, 455–473. https://doi.org/10.1016/0013-4694(49)90219-9.

Newman, M.E., 2002. Assortative mixing in networks. Phys. Rev. Lett. 89, 208701 https://doi.org/10.1103/PhysRevLett.89.208701.

Noirhomme, Q., Brecheisen, R., Lesenfants, D., Antonopoulos, G., Laureys, S., 2017. Look at my classifier's result": disentangling unresponsive from (minimally) conscious

patients. Neuroimage 145, 288–303. https://doi.org/10.1016/j.neuroimage.2015.12.006.
Nuwer, M.R., Comi, G., Emerson, R., Fuglsang-Frederiksen, A., Guerit, J.M., Hinrichs, H., Ikeda, A., Luccas, F.J., Rappelsburger, P., 1998. IFCN standards for digital recording of clinical EEG. International federation of clinical neurophysiology. Electroencephalogr. Clin. Neurophysiol. 106, 259–261. https://doi.org/10.1016/s0013-4694(97)00106-5.
Panda, R., Vanhaudenhuyse, A., Piarulli, A., Annen, J., Demertzi, A., Alnagger, N., Chennu, S., Laureys, S., Faymonville, M.E., Gosseries, O., 2023. Altered brain connectivity and network topological organization in a non-ordinary state of consciousness induced by hypnosis. J. Cogn. Neurosci. 35, 1394–1409. https://doi.org/10.1162/jocn_a_02019.
Penberthy, L.T., Towne, A., Garnett, L.K., Perlin, J.B., DeLorenzo, R.J., 2005. Estimating the economic burden of status epilepticus to the health care system. Seizure 14, 46–51. https://doi.org/10.1016/j.seizure.2004.06.001.
Phang, C.-R., Noman, F., Hussain, H., Ting, C.-M., Ombao, H., 2019. A multi-domain connectome convolutional neural network for identifying schizophrenia from EEG connectivity patterns. IEEE J. Biomed. Health Inform. 24, 1333–1343. https://doi.org/10.1109/JBHI.2019.2941222.
Posner, J.B., Saper, C.B., Schiff, N.D., Jan Claassen, M., 2019. Plum and Posner's diagnosis and Treatment of Stupor and Coma. Oxford University Press, Oxford. https://doi.org/10.1093/med/9780190208875.002.0001.
Power, J.D., Cohen, A.L., Nelson, S.M., Wig, G.S., Barnes, K.A., Church, J.A., Vogel, A.C., Laumann, T.O., Miezin, F.M., Schlaggar, B.L., Petersen, S.E., 2011. Functional network organization of the human brain. Neuron 72, 665–678. https://doi.org/10.1016/j.neuron.2011.09.006.
Refaeilzadeh, P., Tang, L., Liu, H., 2009. Cross-validation. In: Liu, L., Özsu, M.T., Encyclopedia of Database Systems. Springer, New York, NY, pp. 532–538. https://doi.org/10.1007/978-0-387-39940-9_565.
Rivera-Lillo, G., Stamatakis, E.A., Bekinschtein, T.A., Menon, D.K., Chennu, S., 2021. Delta band activity contributes to the identification of command following in disorder of consciousness. Sci. Rep. 11, 16267. https://doi.org/10.1038/s41598-021-95818-6.
Rubinov, M., Sporns, O., 2010. Complex network measures of brain connectivity: uses and interpretations. Neuroimage 52, 1059–1069. https://doi.org/10.1016/j.neuroimage.2009.10.003.
Sanchez-Vives, M.V., Barbero-Castillo, A., Perez-Zabalza, M., Reig, R., 2021. GABA(B) receptors: modulation of thalamocortical dynamics and synaptic plasticity. Neuroscience 456, 131–142. https://doi.org/10.1016/j.neuroscience.2020.03.011.
Schanze, T., Eckhorn, R., 1997. Phase correlation among rhythms present at different frequencies: spectral methods, application to microelectrode recordings from visual cortex and functional implications. Int. J. Psychophysiol. 26, 171–189. https://doi.org/10.1016/s0167-8760(97)00763-0.
Secci, S., Liuzzi, P., Hakiki, B., Burali, R., Draghi, F., Romoli, A.M., di Palma, A., Scarpino, M., Grippo, A., Cecchi, F., Frosini, A., Mannini, A., 2024. Low-density EEG-based functional connectivity discriminates minimally conscious state plus from minus. Clin. Neurophysiol. 163, 197–208. https://doi.org/10.1016/j.clinph.2024.04.021.
Shepherd, G.M.G., Yamawaki, N., 2021. Untangling the cortico-thalamo-cortical loop: cellular pieces of a knotty circuit puzzle. Nat. Rev. Neurosci. 22, 389–406. https://doi.org/10.1038/s41583-021-00459-3.
Shorvon, S., 1994. Status epilepticus: Its Clinical Features and Treatment in Children and Adults. Cambridge University Press, Cambridge. https://doi.org/10.1017/CBO9780511526930.
Simonyan, K., Vedaldi, A., Zisserman, A., 2013. Deep inside convolutional networks: visualising image classification models and saliency maps. arXiv. https://doi.org/10.48550/arXiv.1312.6034.
Stam, C.J., Reijneveld, J.C., 2007. Graph theoretical analysis of complex networks in the brain. Nonlinear Biomed. Phys. 1, 3. https://doi.org/10.1186/1753-4631-1-3.
Sutter, R., Ruegg, S., Kaplan, P.W., 2012. Epidemiology, diagnosis, and management of nonconvulsive status epilepticus: opening Pandora's box. Neurol. Clin. Pract. 2, 275–286. https://doi.org/10.1212/CPJ.0b013e318278be75.
Tan, X., Zhou, Z., Gao, J., Meng, F., Yu, Y., Zhang, J., He, F., Wei, R., Wang, J., Peng, G., Zhang, X., Pan, G., Luo, B., 2019. Structural connectome alterations in patients with disorders of consciousness revealed by 7-tesla magnetic resonance imaging. Neuroimage Clin. 22, 101702 https://doi.org/10.1016/j.nicl.2019.101702.
Thatcher, R.W., Krause, P.J., Hrybyk, M., 1986. Cortico-cortical associations and EEG coherence: a two-compartmental model. Electroencephalogr. Clin. Neurophysiol. 64, 123–143. https://doi.org/10.1016/0013-4694(86)90107-0.
van Diessen, E., Diederen, S.J., Braun, K.P., Jansen, F.E., Stam, C.J., 2013. Functional and structural brain networks in epilepsy: what have we learned? Epilepsia 54, 1855–1865. https://doi.org/10.1111/epi.12350.
Vanhaudenhuyse, A., Noirhomme, Q., Tshibanda, L.J., Bruno, M.A., Boveroux, P., Schnakers, C., Soddu, A., Perlbarg, V., Ledoux, D., Brichant, J.F., Moonen, G., Maquet, P., Greicius, M.D., Laureys, S., Boly, M., 2010. Default network connectivity reflects the level of consciousness in non-communicative brain-damaged patients. Brain 133, 161–171. https://doi.org/10.1093/brain/awp313.
Wang, F., Tian, Y.-C., Zhang, X., Hu, F., 2022. An ensemble of Xgboost models for detecting disorders of consciousness in brain injuries through EEG connectivity. Expert Syst. Appl. 198, 116778 https://doi.org/10.1016/j.eswa.2022.116778.
Yang, H., Wu, H., Kong, L., Luo, W., Xie, Q., Pan, J., Quan, W., Hu, L., Li, D., Wu, X., Liang, H., Qin, P., 2024. Precise detection of awareness in disorders of consciousness using deep learning framework. Neuroimage 290, 120580. https://doi.org/10.1016/j.neuroimage.2024.120580.
Yang, Y., Dai, Y., He, Q., Wang, S., Chen, X., Geng, X., He, J., Duan, F., 2023. Altered brain functional connectivity in vegetative state and minimally conscious state. Front. Aging Neurosci. 15, 1213904 https://doi.org/10.3389/fnagi.2023.1213904.
Yang, Z.T., Chen, H.J., Chen, Q.F., Lin, H., 2018. Disrupted brain intrinsic networks and executive dysfunction in cirrhotic patients without overt hepatic encephalopathy. Front. Neurol. 9, 14. https://doi.org/10.3389/fneur.2018.00014.
Zamani, N., Hassanian-Moghaddam, H., Zamani, N., 2022. Strategies for the treatment of acute benzodiazepine toxicity in a clinical setting: the role of antidotes. Expert Opin. Drug Metab. Toxicol. 18, 367–379. https://doi.org/10.1080/17425255.2022.2105692.
Zehtabchi, S., Abdel Baki, S.G., Omurtag, A., Sinert, R., Chari, G., Malhotra, S., Weedon, J., Fenton, A.A., Grant, A.C., 2013. Prevalence of non-convulsive seizure and other electroencephalographic abnormalities in ED patients with altered mental status. Am. J. Emerg. Med. 31, 1578–1582. https://doi.org/10.1016/j.ajem.2013.08.002.
Zhou, J., Liu, X., Song, W., Yang, Y., Zhao, Z., Ling, F., Hudetz, A.G., Li, S.J., 2011. Specific and nonspecific thalamocortical functional connectivity in normal and vegetative states. Conscious. Cogn. 20, 257–268. https://doi.org/10.1016/j.concog.2010.08.003.